Density dependence of the excitation gaps in an undoped Si/SiGe double-quantum-well heterostructure

D. Chen, S. Cai, N.-W. Hsu, et al.

View Online   Export Citation   CrossMark

ARTICLES YOU MAY BE INTERESTED IN

Density dependence of the excitation gaps in an undoped Si/SiGe double-quantum-well heterostructure

D. Chen,[1] S. Cai,[1] N.-W. Hsu,[2] S.-H. Huang,[2] Y. Chuang,[2] E. Nielsen,[3] J.-Y. Li,[2,4] (iD) C. W. Liu,[2] (iD) T. M. Lu,[3] (iD) and D. Laroche[1,a) (iD)

AFFILIATIONS

[1]Department of Physics, University of Florida, Gainesville, Florida 32611, USA
[2]Department of Electrical Engineering and Graduate Institute of Electronic Engineering, National Taiwan University, Taipei 10617, Taiwan
[3]Sandia National Laboratories, Albuquerque, New Mexico 87185, USA
[4]Taiwan Semiconductor Research Institute, Hsinchu 30078, Taiwan

a)Author to whom correspondence should be addressed: dlaroc10@ufl.edu

ABSTRACT

We report low-temperature magneto-transport measurements of an undoped Si/SiGe asymmetric double quantum well heterostructure. The density in both layers is tuned independently utilizing top and bottom gates, allowing the investigation of quantum wells at both imbalanced and matched densities. Integer quantum Hall states at total filling factor $\nu_T = 1$ and $\nu_T = 2$ are observed in both density regimes, and the evolution of their excitation gaps is reported as a function of the density. The $\nu_T = 1$ gap evolution departs from the behavior generally observed for valley splitting in the single layer regime. Furthermore, by comparing the $\nu_T = 2$ gap to the single particle tunneling energy, Δ_{SAS}, obtained from Schrödinger–Poisson (SP) simulations, evidence for the onset of spontaneous interlayer coherence is observed for a relative filling fraction imbalance smaller than $\sim$50%.

Published under an exclusive license by AIP Publishing. https://doi.org/10.1063/5.0068538

Owing to their compatibility with the widespread complementary metal-oxide-semiconductor (CMOS) technology enabling a scalable and affordable fabrication process, Si-based heterostructures continue to attract a lot of attention for both fundamental and applied research.[1] In particular, the substantial low-temperature mobility improvements achieved in SiGe-based heterostructures[2] have enabled various studies of low-disorder phenomena such as the fractional quantum hall effect,[3] valley splitting,[4–6] quantum dots,[7–9] as well as long lifetime and high fidelity electron spin qubits[10,11] that are predominantly studied alongside GaAs-[12,13] and graphene-based[14,15] devices.

The vast majority of the experimental efforts on quantum transport in SiGe-based heterostructures have focused on the development and characterization of single layer devices, while coupled Si/SiGe bilayers[16,17] have received little attention. However, bilayer systems present a promising platform in their own right for studying interlayer coherence and the onset of indirect exciton condensation.[18–22] In addition, the evolution of valley splitting in Si/SiGe bilayers is of crucial interest for the realization of long-lived silicon spin qubits.[23] Undoped

Si/SiGe double quantum wells have only been investigated in top-gated devices,[17] severely limiting the density tunability of the devices' bottom well. Unlike these prior studies, the device presented in this Letter hosts a bilayer system that is dual-gated, allowing independent control of the density in both layers simultaneously. Utilizing this enhanced control, the evolution of the density dependence of the excitation gaps at total filling fractions $\nu_T = 1$ and $\nu_T = 2$ is reported both at mismatched and matched densities.

Closely following previous heterostructure designs,[17] the double-quantum well structure presented in this Letter was designed to contain a 5 nm top quantum well, a 2 nm $Si_{0.72}Ge_{0.28}$ interwell barrier, and a 15 nm bottom quantum well. In contrast to the previous structure, the interwell barrier's Ge content was increased to 28% to suppress tunneling between the two wells. The heterostructure was grown in an ultra-high-vacuum chemical vapor-deposition system with Si H_4 and Ge H_4 as precursors on a p-type Si substrate. As depicted in Fig. 1(a), the layer composition is, from bottom to top: a graded SiGe virtual substrate with a maximal Ge composition of 14%, a $\sim$3 μm thick
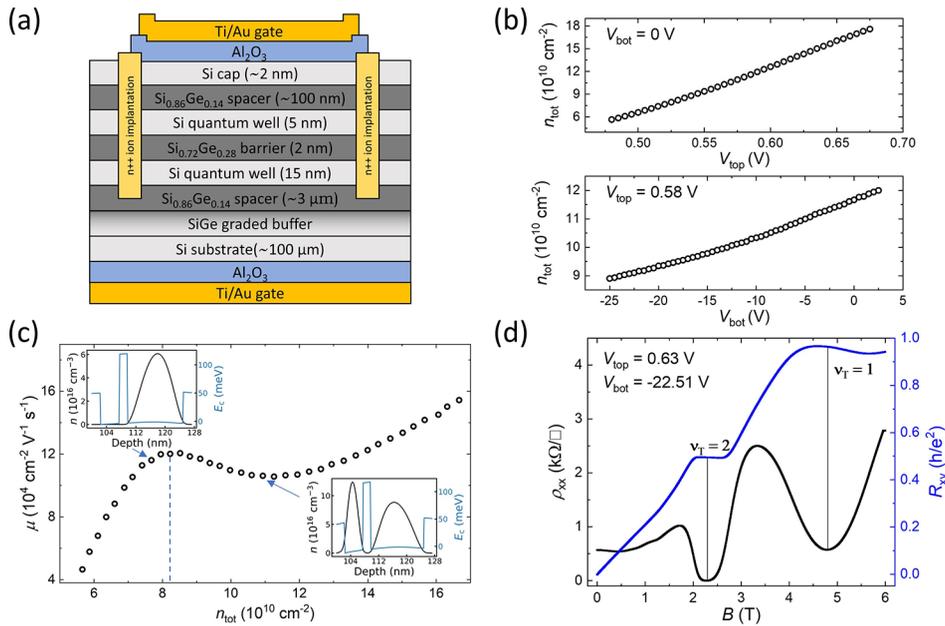
FIG. 1. (a) Complete layer schematic of the device. (b) Top panel: Total density dependence vs top gate voltage with the bottom gate voltage set to 0. Bottom panel: Total density dependence vs bottom gate voltage with a top gate voltage of 0.58 V. (c) Total 2D density vs mobility dependence at fixed $V_{bot} = 0$ V. A similar plot over a wider density range is shown in the supplementary material. Top left (right) inset: SP simulation results describing the band diagram and 3D electron density distribution below (above) $n_{crossover}$, the blue dotted line in the main panel. (d) Hall resistance (blue) and longitudinal resistivity (black) as a function of the magnetic field for $V_{top} = 0.63$ V and $V_{bot} = -22.51$ V. The top and bottom wells' densities are 5.41×10^{10} and 5.82×10^{10} cm^{-2}, respectively. The method to extract each layers' densities is detailed in the supplementary material.

relaxed $Si/Si_{0.86}Ge_{0.14}$ spacer layer, the (strained) double quantum well structure described above, an additional $\sim100\,\mu m$ $Si/Si_{0.86}Ge_{0.14}$ spacer layer, and a 2 nm Si cap.

The asymmetric (AS) quantum well structure ensures that, in the uncoupled limit, the ground state energies in the two wells are different. Thus, during top gate operations, a sizable electron density can accumulate in the wider bottom layer before electrons start to populate the top layer, drastically reducing further electron accumulation in the bottom layer through screening. Such a design is necessary owing to the large separation, $\sim100\,\mu m$, between the bottom gate and the bottom quantum well, limiting the degree of density tuning achievable from the bottom gate alone.

To enable electrical measurements on the bilayer, a heterostructure field-effect transistor (HFET) was patterned following standard fabrication processes described in detail in a previous Letter.[17] First, heavy phosphorus ion implantation was used for Ohmic contacts. Prior to the deposition of the Hall bar-shaped Ti/Au gate, 1000 cycles of atomic-layer-deposited Al_2O_3 were grown. Finally, the back Ti/Au gate was implemented by mechanically lapping the substrate down to $\sim100\,\mu m$, followed by a similar oxide and metal deposition scheme.

The device was tested in a cryo-free Blue Fors dilution refrigerator with a base temperature of $T \sim 10$ mK. Standard low-frequency (37.3 Hz) lock-in measurement techniques were used in a four-terminal geometry with a constant 50 nA excitation current. Prior to the initial operation of the device, a large negative bias (-7 V) was applied to evacuate negative charges trapped at the dielectric layer interface, improving device reliability. The measurements were found to be consistent over several thermal cycles.

The Hall density of the device is extracted from the slope of the Hall resistance (R_{xy}) at small magnetic fields ($B \leq 0.1$ T), and its dependence on the top (bottom) gate voltage at $V_{bot} = 0$ V ($V_{top} = 0.58$ V) is shown in the top (bottom) panel of Fig. 1(b). Both curves show near-linear behavior, while the bottom gate voltage

dependence has a smaller slope owing to a larger gate-to-well separation.

Total Hall densities were tuned from 6.8×10^{10} to 34.2×10^{10} cm^{-2} with a maximal Hall mobility of 30.8×10^4 cm$^2/(V\,s)$ achieved at the highest density. The crossover density (the electronic density required to start populating the top quantum well) was observed at $n_{crossover} = 8.22 \times 10^{10}$ cm^{-2}. Identification of $n_{crossover}$ and confirmation of bilayer behavior are assessed from the mobility drop in the density vs mobility plot, caused by interlayer scattering,[24] as exemplified in the main panel of Fig. 1(c).

The experimental crossover density was also replicated using an iterative, self-consistent Schrödinger–Poisson (SP) simulation. Using the nominal growth parameters and thicknesses, the experimental crossover density was reproduced via the simulation by shifting the lower boundary condition, corresponding to a constant offset in the bottom gate voltage. The insets of Fig. 1(c) illustrate the simulated band diagram and electron density distribution before and after $n_{crossover}$. To prevent charge accumulation at either interface, the conduction band of the upper (lower) half of the heterostructure's top (bottom) spacer is artificially increased to be 500 meV above that of the quantum wells.[17] We also note that it was possible to reproduce the experimental crossover density without utilizing a bottom gate voltage offset by considering a modified structure with a top well width of 3.8 nm, an interlayer barrier of 2.2 nm, and a bottom well width of 15 nm.

Two density regimes are studied in this Letter. The variable imbalanced density regime describes experimental conditions where only V_{top} is increased from 0 to positive values, while V_{bot} is fixed at 0 V, as exemplified in Fig. 1(c). Beyond $n_{crossover}$, the density in the top layer steadily increases toward matched densities, while the density in the bottom layer remains nearly constant, changing by less than 4% according to simulations. In contrast, both gates are biased in the matched density regime, yielding densities within 6% of one another

in each layer, under the assumption of ideal gate screening by the 2DEGs. Independent contacts to both layers or a capacitive measurement scheme[25] would be needed to further refine this estimate. Details on the tuning scheme can be found in the supplementary material. An instance of the latter case is shown in Fig. 1(d), where the traces of the Hall resistance, R_{xy}, and of the longitudinal resistivity, ρ_{xx}, at a front gate voltage of $V_{top} = 0.63$ V and a back gate voltage of $V_{bot} = -22.51$ V are presented. In both regimes, the data clearly exhibit quantum Hall plateaus developing at $\nu_T = 1$ and $\nu_T = 2$ within 3% of h/e^2.

The evolution of ρ_{xx} as a function of the magnetic field and total density is presented in Fig. 2 for both variable imbalanced (a) and matched (c) densities. Quantum Hall plateaus are clearly observed for $\nu_T = 1$ and $\nu_T = 2$, indicated by dotted yellow lines. Although less developed, the $\nu_T = 4$ minima are also observed.

The main results of this Letter are presented in Figs. 2(b) and 2(d), where the quantum Hall excitation gaps, extracted from the temperature dependence of the ρ_{xx} minima, are shown for the variable imbalanced and matched density regimes, respectively. The inset in Fig. 2(d) shows a typical example of the dependence ρ_{xx} has on the temperature in an Arrhenius plot. The linear part of the plot was systematically determined and fitted to an activation model,[26] and the extracted slope was used to determine the excitation gap Δ: $\rho_{xx}(T) = \rho_0 e^{-\Delta/2T}$. The deviation from linearity at low temperatures is attributed to interstitial hopping.[27] The shaded confidence intervals in the main panel are determined from either adding and/or subtracting an additional point to/from the determined linear activation interval, whenever possible. For additional details on the fitting procedure, see the supplementary material.

In the single layer regime, strained Si contains two degeneracies per Landau level: spins ($\uparrow\downarrow$) and valleys ($\pm$). For $n_{tot} = 10 \times 10^{10}$ cm^{-2}, the single layer valley splitting is estimated to be ~1.35 K at 4.13 T.[28] At the same magnetic field, the spin gap would be ~2.79 K without considering many-body effects. This implies that the $\nu_T = 1$ ($\nu_T = 2$) state is associated with the valley (spin) degree of freedom. Upon entering the bilayer regime, an additional degeneracy, the layer degree of freedom (S/AS), comes into play. The tunneling gap, Δ_{SAS},[26] characterizing this degeneracy can be estimated from the SP simulation. As we do not observe Landau level crossing in our magneto-transport measurements [Fig. 2(a)], we can safely attribute the bilayer $\nu_T = 1$ state to valley splitting. The $\nu_T = 2$ state is attributed either to spin-splitting or to interlayer effects. In the latter case, two mechanisms can give rise to the quantum Hall state: a single-particle state caused by interlayer tunneling[26,29] or a many-body state resulting from spontaneous interlayer coherence (SIC).[29–31]

Although valley splitting in vertically coupled Si/SiGe bilayers has not been investigated yet, the single layer regime has attracted a lot of interest both experimentally[23,32] and theoretically.[33,34] For single layers, the conduction band valley degeneracy is lifted by a sharp quantum well interface. Atomic-scale disorder, attributed to random SiGe alloys and steps in the quantum well, causes destructive interference that suppresses valley splitting. Theoretical calculations predict a linear dependence that extrapolates to a value that coincides with sample-dependent Landau level disorder broadening at zero density.[34]

The evolution of the $\nu_T = 1$ gap in the single layer regime, presented in red in Fig. 2(b), follows these expectations. Linearly fitting the data below $n_{crossover}$, we obtain an estimate for the disorder broadening $\Gamma \sim 0.327$ K and for a linear coefficient $c_B \sim 0.29$ K/T,
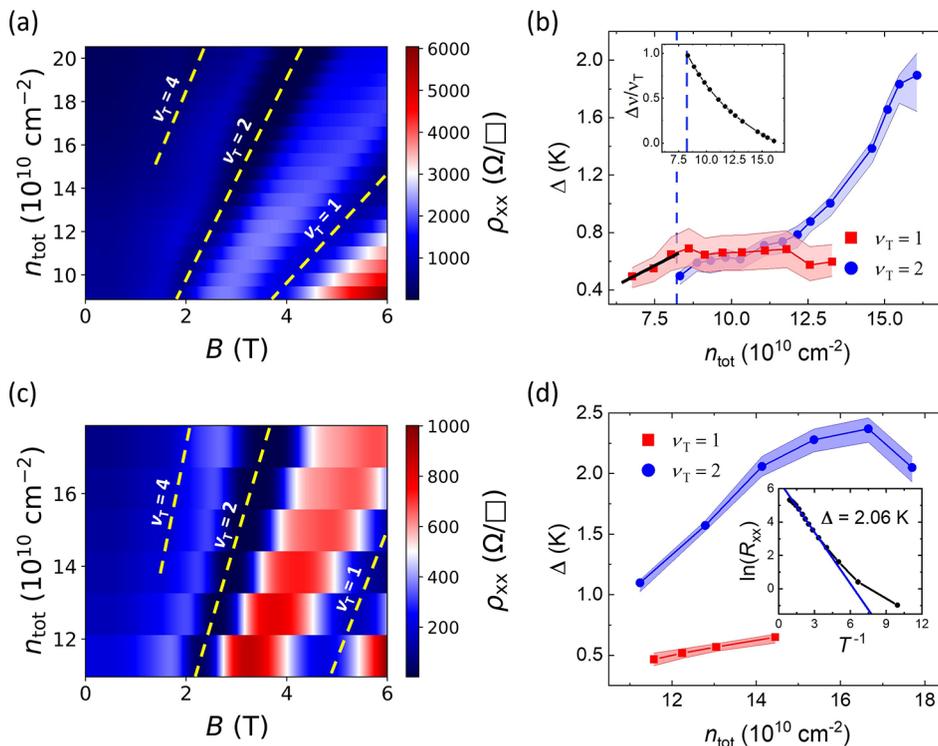
FIG. 2. (a) 2D color map exhibiting the longitudinal resistivity, ρ_{xx} as a function of n_{tot} and B for variable imbalanced densities. The matched density case is shown in panel (c). (b) Density dependence of the extracted activation gaps at variable imbalanced densities with confidence intervals for $\nu_T = 1$ (red squares) and $\nu_T = 2$ (blue circles). $n_{crossover}$ is indicated by the blue dotted line. In addition, a black line indicates the points used to fit the estimated disorder broadening, Γ, and the linear valley splitting coefficient, c_B. The matched density case is shown in panel (d). Inset (b): Relative filling fraction imbalance as a function of the total density (same scale as main graph) for the variable imbalanced density case. As the bottom well's density marginally increases beyond the crossover density, the top layer's density slowly catches up to the bottom layer's density, thereby reducing the filling fraction imbalance. Inset (d): Temperature dependence of the ρ_{xx} minima in an Arrhenius plot for $\nu_T = 2$ at $V_{top} = 0.64$ V and $V_{bot} = -12.368$ V in the matched density regime.

consistent with previous studies in Si/SiGe heterostructures reporting similar results:[28] $\Gamma \sim 0.435$ K and $c_B \sim 0.326$ K/T. However, this behavior changes drastically in the bilayer regime. The single layer linear dependence strongly decreases and nearly flattens out. This remains true in the matched density case where the linear coefficient is nearly reduced by a factor of 2 to $c_B \sim 0.15$ K/T. Further theoretical and experimental studies of this unexpected behavior are required to determine whether Si bilayers exhibit large valley splitting at low magnetic fields or even spontaneous valley polarization.[33,35]

To understand the evolution of the $\nu_T = 2$ state, one has to consider the interplay between spin-splitting and interlayer effects. One interlayer mechanism that may induce the $\nu_T = 2$ quantum Hall state in coherent bilayers[18] occurs when the tunneling between the two quantum wells is sufficiently strong, resulting in an overlap of the wave functions in each well. As a result, the individual layer eigenstates hybridize into symmetric and antisymmetric states with single-particle tunnel splitting gap, $\Delta_{SAS} = E_{AS} - E_S$.[36] Δ_{SAS} depends strongly on the height and width of the interwell barrier.

Spontaneous interlayer coherence (SIC) is another interlayer mechanism that can give rise to the $\nu_T = 2$ state. As a signature of exciton condensation between spatially separated electrons and holes, SIC induces a coherent state that can occur solely due to Coulomb interactions in the limit of low interlayer tunneling; when the ratio between interlayer and intralayer Coulomb interactions is less than a critical value: $d/l_b \lesssim 1.8$.[37,38] Here, d is the distance between the centers of each quantum well, and $l_b = (\hbar/eB)^{1/2}$ is the magnetic length. The device reported in this Letter has d/l_b values ranging between 0.62 and 1.24, well within the range where SIC can be observed. Furthermore, the ratio of the SP simulated Δ_{SAS} gap to the Coulomb

energy ($e^2/\epsilon l_b$) is $\sim 5 \times 10^{-4}$, indicating that the device is indeed in the Coulomb dominated regime.

Both spin-splitting and interlayer tunneling are captured within the SP simulations. In addition to the two different cases used to reproduce $n_{crossover}$, two different interwell barrier heights, ϕ_b, were used. The first one corresponds to a Ge content of 28.8 %, giving $\phi_b = 141.2$ meV; while the other assumes a 25.8% Ge content, giving $\phi_b = 122.8$ meV.[39] Together, we have, thus, simulated four cases. We note that further increasing the Ge content of the barrier would have negligible effects on its height. Only the case with as-grown parameters and higher interwell barriers is shown in Fig. 3. The other three cases are shown in the supplementary material. The general shape of the density dependence of Δ_{SAS} is nearly identical in all four cases. However, the magnitude of Δ_{SAS} can be up to $\sim 96\%$ larger for the case of thinner top well widths and weaker interlayer barriers, as opposed to as-grown parameters and higher interwell barriers. Panel (a) [panel (c)] of Fig. 3 depicts the evolution of the energy fan diagrams for the variable imbalanced (matched) density regime. Here, only spin splitting and Δ_{SAS} are considered while valley splitting is omitted from the calculations, resulting in four energy sub-levels per Landau level. As such, the simulation strictly provides information about E_{2n}, the energy of the even quantum Hall states. The yellow shaded regions denote the simulated E_2. The simulated second Landau energy level, E_2, for the variable imbalanced density case is also shown in Fig. 3(b), while the simulated Δ_{SAS} for the matched density case is shown in Fig. 3(d).

From theory,[28] we expect the experimental gap to be $\Delta_2 = E_2 - E_1 - \Gamma = E_2 - \Delta_1 - 2\Gamma$. In the variable imbalanced density case at low densities, the simulated E_2 and the experimentally
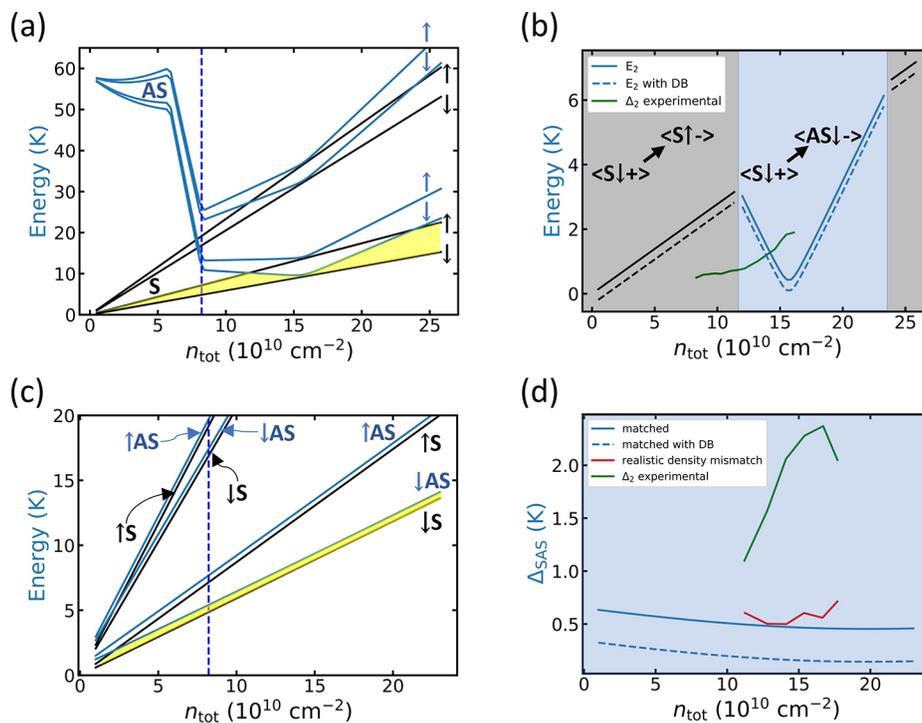
FIG. 3. (a) Simulated energy fan diagram depicting the 0th and first Landau levels for variable imbalanced densities. The matched density case is shown in panel (c). The symmetric (S) state subband is shown as black lines while the asymmetric (AS) state subband is shown as blue lines. Spin is denoted by arrows. The dotted line indicates where $n_{crossover}$ occurs. Valley splitting is omitted from the calculations. The yellow shaded regions indicate the energy gaps considered for panel (b) and (d). (b) As a function of the density, E_2 can either result from a spin state transition (shaded black) or from a layer state transition (shaded blue). (d) Δ_{SAS} values for exactly matched densities (blue) and for the slightly mismatched densities measured experimentally (red); see Table S.I. in the supplementary material. The dotted lines in panels (b) and (d) take into consideration disorder broadening. The experimentally measured $\nu_T = 2$ excitation gaps are shown as green lines in panels (b) and (d).

measured Δ_2 are similar. Starting in the single layer regime, a linear dependence is observed as long as E_2 originates from a spin state transition. A downturn in the gap magnitude is then observed with increasing density once the state originates from Δ_{SAS}. However, the measured magnitude of Δ_2 is notably smaller than the simulated E_2. In addition, the theoretical downturn in E_2 is reduced to the point of flattening, and its experimental onset occurs at a reduced density, 9.8×10^{10} cm^{-2}. As shown in Fig. 3(b), disorder broadening alone cannot explain the observed discrepancy. A non-linearity of the valley splitting excitation gap, Δ_1, might explain this discrepancy, but the same non-linearity prevents us from extrapolating the experimentally measured Δ_1 to lower densities and magnetic fields.

At higher densities, the behavior of Δ_2 departs more strongly from the simulated E_2, shown in Fig. 3(b). The downturn is rapidly inverted, and the overall magnitude of Δ_2 overtakes that of the disorder-broadening corrected Δ_{SAS} as the layers approach matched densities, where Δ_{SAS} is calculated to be at its weakest. Both the qualitative departure from the Δ_{SAS} density dependence as well as the increased Δ_2 value are consistent with the onset of SIC.[30] This is further confirmed by the behavior of Δ_2 in the density matched case [Fig. 2(d)]. Here, Δ_2 has a concavity opposite to that of Δ_{SAS} [Fig. 3(d)] and a magnitude of up to ten times larger than that of the disorder-broadened Δ_{SAS}, at $\Delta_2 = 2.37$ K. Overall, the SP simulations show that neither Δ_{SAS}, spin-splitting nor Landau level spacing alone reproduces the qualitative behavior obtained experimentally. Extrapolating the density dependence of Δ_1 to lower magnetic fields is also insufficient to account for the differences between the measured Δ_2 and the simulated Δ_{SAS}.

Considering the density imbalance between the layers, shown in the inset of Fig. 2(b), the onset of Δ_2's magnitude increase coincides with a relative density imbalance $\frac{\Delta\nu}{\nu_T} = \frac{\nu_1 - \nu_2}{2} \approx 0.5$ at $n_{tot} = 11.07 \times 10^{10}$ cm^{-2}. Prior studies in GaAs bilayers[40,41] have reported that SIC remains intact for relative density imbalances as large as $\frac{\Delta\nu}{\nu_T} = 0.5$, which is in quantitative agreement with our observations.

Three main parameters influence the strength of Δ_2 induced by SIC: The interlayer to intralayer Coulomb interactions ratio, d/l_b, the tunneling strength Δ_{SAS}, and the density imbalance $\Delta\nu$. As the total density is increased in our device, d/l_b increases while Δ_{SAS} decreases. $\Delta\nu$ also decreases for the density imbalanced regime. While the excitation gap has previously been shown to increase with decreasing d/l_b[29,30] and increasing $\Delta\nu$,[41–44] tunneling has been shown to weaken the SIC induced quantum state.[29,45] Therefore, we attribute the increase in Δ_2 with increasing density to the reduced tunneling. Indeed, going toward higher density decreases tunneling as the wave functions are pushed farther apart. The downturn of Δ_2 at the highest densities in the matched density case coincides with the saturation of the simulated Δ_{SAS} [Fig. 3(d)] and can be explained by the increased d/l_b at constant tunneling. These effects are likely noticeable in our device since tunneling ($\Delta_{SAS} \geq 500$ m K) is over 1000 times larger than prior studies probing similar effects.[42,43,46] While our observations are consistent with a SIC-induced Δ_2, we cannot fully rule out that a significant reduction of valley splitting at lower magnetic fields is at the origin of this phenomenon since the value of Δ_1 at $B \sim 2$ T is neither know experimentally nor theoretically.

In conclusion, we have fabricated and performed magneto-transport measurements on a novel back-gated Si/SiGe bilayer system. The density dependence of the excitation gaps for $\nu_T = 1$ and $\nu_T = 2$ has been studied in both the variable imbalanced and matched density regimes and has been compared to values obtained from SP simulations. The $\nu_T = 1$ state is attributed to valley-splitting while the $\nu_T = 2$ state is attributed to spin-splitting at low densities and interlayer effects at larger density. Stark departure in the density evolution of the $\nu_T = 1$ excitation gap between the single and bilayer regimes has been reported, highlighting the need for theoretical work on valley splitting in bilayer Si/SiGe structures. Evidence for exciton condensation has been observed in the $\nu_T = 2$ state for $\frac{\Delta\nu}{\nu_T} < 0.5$. Achieving independent contacts to both layers in order to perform tunneling conductance,[37] Coulomb drag,[38] and counterflow measurements[19,47] would be required to further confirm this conclusion. Reducing the separation between the bottom quantum well and the bottom gate as well as utilizing larger magnetic fields would enable studies of these effects over a wider density range. These results highlight the prospects of Si/SiGe bilayers as a platform for valley splitting tuning and exciton condensation, which may have potential applications toward realizing SiGe-based[48] or Bose–Einstein condensate based[49] qubits.

See the supplementary material for details on the methods used to achieve matched density between the layers, how to extract the excitation gaps, as well as results from the four cases used in the SP simulations.

AUTHOR DECLARATIONS
Conflict of Interest

The authors have no conflicts to disclose.

DATA AVAILABILITY

The data that support the findings of this study are openly available in IR@UF, Ref. No. IR00011549.

REFERENCES

[1]K. K. Ng, *Complete Guide to Semiconductor Devices* (IEEE Press, 2002).
[2]T. Lu, D. Tsui, C.-H. Lee, and C. Liu, Appl. Phys. Lett. **94**, 182102 (2009).
[3]T. Lu, W. Pan, D. Tsui, C.-H. Lee, and C. Liu, Phys. Rev. B **85**, 121307 (2012).
[4]P. Weitz, R. Haug, K. V. Klitzing, and F. Schäffler, Surf. Sci. **361–362**, 542 (1996).

[5]S. F. Neyens, R. H. Foote, B. Thorgrimsson, T. Knapp, T. McJunkin, L. Vandersypen, P. Amin, N. K. Thomas, J. S. Clarke, D. Savage *et al.*, Appl. Phys. Lett. **112**, 243107 (2018).

[6]T. McJunkin, E. R. MacQuarrie, L. Tom, S. F. Neyens, J. P. Dodson, B. Thorgrimsson, J. Corrigan, H. E. Ercan, D. E. Savage, M. G. Lagally, R. Joynt, S. N. Coppersmith, M. Friesen, and M. A. Eriksson, Phys. Rev. B **104**, 085406 (2021).

[7]X. Xue, T. Watson, J. Helsen, D. R. Ward, D. E. Savage, M. G. Lagally, S. N. Coppersmith, M. Eriksson, S. Wehner, and L. Vandersypen, Phys. Rev. X **9**, 021011 (2019).

[8]A. Mills, D. Zajac, M. Gullans, F. Schupp, T. Hazard, and J. Petta, Nat. Commun. **10**(1), 1063 (2019).

[9]W. Lawrie, H. Eenink, N. Hendrickx, J. Boter, L. Petit, S. Amitonov, M. Lodari, B. Paquelet Wuetz, C. Volk, S. Philips *et al.*, Appl. Phys. Lett. **116**, 080501 (2020).

[10]C. Simmons, J. Prance, B. Van Bael, T. S. Koh, Z. Shi, D. Savage, M. Lagally, R. Joynt, M. Friesen, S. Coppersmith *et al.*, Phys. Rev. Lett. **106**, 156804 (2011).

[11]M. Russ, D. M. Zajac, A. J. Sigillito, F. Borjans, J. M. Taylor, J. R. Petta, and G. Burkard, Phys. Rev. B **97**, 085421 (2018).

[12]J. R. Petta, A. C. Johnson, J. M. Taylor, E. A. Laird, A. Yacoby, M. D. Lukin, C. M. Marcus, M. P. Hanson, and A. C. Gossard, Science **309**, 2180 (2005).

[13]S. D. Sarma and A. Pinczuk, *Perspectives in Quantum Hall Effects: Novel Quantum Liquids in Low-Dimensional Semiconductor Structures* (John Wiley & Sons, 2008).

[14]K. I. Bolotin, F. Ghahari, M. D. Shulman, H. L. Stormer, and P. Kim, Nature **462**, 196 (2009).

[15]Y. Shimazaki, M. Yamamoto, I. V. Borzenets, K. Watanabe, T. Taniguchi, and S. Tarucha, Nat. Phys. **11**, 1032 (2015).

[16]H. Malissa, D. Gruber, D. Pachinger, F. Schäffler, W. Jantsch, and Z. Wilamowski, Superlattices Microstruct. **39**, 414 (2006).

[17]D. Laroche, S.-H. Huang, E. Nielsen, C. W. Liu, J.-Y. Li, and T.-M. Lu, Appl. Phys. Lett. **106**, 143503 (2015).

[18]J. Eisenstein, G. Boebinger, L. Pfeiffer, K. West, and S. He, Phys. Rev. Lett. **68**, 1383 (1992).

[19]E. Tutuc, M. Shayegan, and D. Huse, Phys. Rev. Lett. **93**, 036802 (2004).

[20]L. Tiemann, W. Dietsche, M. Hauser, and K. Von Klitzing, New J. Phys. **10**, 045018 (2008).

[21]G. W. Burg, N. Prasad, B. Fallahazad, A. Valsaraj, K. Kim, T. Taniguchi, K. Watanabe, Q. Wang, M. J. Kim, L. F. Register *et al.*, Nano Lett. **17**, 3919 (2017).

[22]J. Li, T. Taniguchi, K. Watanabe, J. Hone, and C. Dean, Nat. Phys. **13**, 751 (2017).

[23]S. Goswami, K. Slinker, M. Friesen, L. McGuire, J. Truitt, C. Tahan, L. Klein, J. Chu, P. Mooney, D. W. Van Der Weide *et al.*, Nat. Phys. **3**, 41 (2007).

[24]H. Störmer, A. Gossard, and W. Wiegmann, Solid State Commun. **41**, 707 (1982).

[25]S. Dorozhkin, A. Kapustin, I. Fedorov, V. Umansky, K. V. Klitzing, and J. Smet, J. Appl. Phys. **123**, 084301 (2018).

[26]G. Boebinger, H. Jiang, L. Pfeiffer, and K. West, Phys. Rev. Lett. **64**, 1793 (1990).

[27]G. Ebert, K. V. Klitzing, C. Probst, E. Schuberth, K. Ploog, and G. Weimann, Solid State Commun. **45**, 625 (1983).

[28]B. P. Wuetz, M. P. Losert, A. Tosato, M. Lodari, P. L. Bavdaz, L. Stehouwer, P. Amin, J. S. Clarke, S. N. Coppersmith, A. Sammak *et al.*, Phys. Rev. Lett. **125**, 186801 (2020).

[29]S. He, S. D. Sarma, and X. Xie, Phys. Rev. B **47**, 4394 (1993).

[30]S. Murphy, J. Eisenstein, G. Boebinger, L. Pfeiffer, and K. West, Phys. Rev. Lett. **72**, 728 (1994).

[31]A. Sawada, Z. Ezawa, H. Ohno, Y. Horikoshi, Y. Ohno, S. Kishimoto, F. Matsukura, M. Yasumoto, and A. Urayama, Phys. Rev. Lett. **80**, 4534 (1998).

[32]K. Lai, W. Pan, D. Tsui, S. Lyon, M. Mühlberger, and F. Schäffler, Phys. Rev. Lett. **93**, 156805 (2004).

[33]M. Friesen, M. Eriksson, and S. Coppersmith, Appl. Phys. Lett. **89**, 202106 (2006).

[34]M. Friesen, S. Chutia, C. Tahan, and S. Coppersmith, Phys. Rev. B **75**, 115318 (2007).

[35]M. S. Hossain, M. Ma, K. Rosales, Y. Chung, L. Pfeiffer, K. West, K. Baldwin, and M. Shayegan, arXiv:2011.06721 (2020).

[36]J. Hu and A. MacDonald, Phys. Rev. B **46**, 12554 (1992).

[37]I. Spielman, J. Eisenstein, L. Pfeiffer, and K. West, Phys. Rev. Lett. **84**, 5808 (2000).

[38]M. Kellogg, I. Spielman, J. Eisenstein, L. Pfeiffer, and K. West, Phys. Rev. Lett. **88**, 126804 (2002).

[39]F. Schäffler, Semicond. Sci. Technol. **12**, 1515 (1997).

[40]I. Spielman, M. Kellogg, J. Eisenstein, L. Pfeiffer, and K. West, Phys. Rev. B **70**, 081303 (2004).

[41]A. Champagne, A. Finck, J. Eisenstein, L. Pfeiffer, and K. West, Phys. Rev. B **78**, 205310 (2008).

[42]E. Tutuc, S. Melinte, E. De Poortere, R. Pillarisetty, and M. Shayegan, Phys. Rev. Lett. **91**, 076802 (2003).

[43]W. Clarke, A. Micolich, A. Hamilton, M. Simmons, C. B. Hanna, J. Rodriguez, M. Pepper, and D. Ritchie, Phys. Rev. B **71**, 081304 (2005).

[44]R. Wiersma, J. Lok, W. Dietsche, K. v Klitzing, D. Schuh, and W. Wegscheider, Phys. Status Solidi B **243**, 3643 (2006).

[45]T. Lay, Y. Suen, H. Manoharan, X. Ying, M. Santos, and M. Shayegan, Phys. Rev. B **50**, 17725 (1994).

[46]D. Zhang, S. Schmult, V. Venkatachalam, W. Dietsche, A. Yacoby, K. von Klitzing, and J. Smet, Phys. Rev. B **87**, 205304 (2013).

[47]Y. Yoon, L. Tiemann, S. Schmult, W. Dietsche, K. von Klitzing, and W. Wegscheider, Phys. Rev. Lett. **104**, 116802 (2010).

[48]Y. Xu, F. Unseld, A. Corna, A. Zwerver, A. Sammak, D. Brousse, N. Samkharadze, S. Amitonov, M. Veldhorst, G. Scappucci *et al.*, Appl. Phys. Lett. **117**, 144002 (2020).

[49]T. Byrnes, K. Wen, and Y. Yamamoto, Phys. Rev. A **85**, 040306 (2012).